Chemistry–A European Journal
Research Article
doi.org/10.1002/chem.202303860
Chemistry Europe
European Chemical Societies Publishing
www.chemeurj.org

The impact of stoichiometry on the initial steps of crystal formation: Stability and lifetime of charged triple-ion complexes

Janou A. Koskamp,[a] Sergěj Y. M. H. Seepma,[a] Vincent F. D. Peters,[a] Dimitrios Toroz,[b] Devis Di Tommaso,[b] and Mariette Wolthers*[a]

Minerals form in natural systems from solutions with varying ratios of their lattice ions, yet non-stoichiometric conditions have generally been overlooked in investigations of new formation (nucleation) of ionic crystals. Here, we investigated the influence of cation:anion ratio in the solution on the initial steps of nucleation by studying positively and negatively charged triple ion complexes and subsequent particle size evolution. Our model systems are carbonates and sulfates of calcium and barium, as it was recently shown that solution stoichiometry affects the timing and rate of their nucleation. Molecular dynamics (MD) simulations and dynamic light scattering (DLS) flow experiments show that nucleation correlates with the stability and lifetime of the initial complexes, which were significantly impacted by the cation:anion stoichiometry and ion type. Specifically, $Ba(SO_4)_2^{2-}$ was found to have higher association constants and its lifetime was twofold longer than $Ba_2SO_4^{2+}$. Similar trends were observed for $BaCO_3$ and $CaSO_4$. Contrastingly, for $CaCO_3$, $Ca(CO_3)_2^{2-}$ was found to have lower association constants and its lifetime was shorter than $Ca_2CO_3^{2+}$. These trends in stability and lifetime follow the same asymmetrical behaviour as observed experimentally for particle formation using techniques like DLS. This suggests a causal relationship between the stability and lifetime of the initial charged complexes and the nucleation under non-stoichiometric conditions.

Introduction

When mineral nucleation experiments are conducted in solutions with ideal ionic ratio, i.e., the cation:anion stoichiometric ratio of the uncharged final crystal, the most abundant nuclei that form are charge neutral.[1–3] Their formation can be described with nucleation theories based on uncharged gas condensation into droplets.[4] This was the basis for the classical nucleation theory (CNT, see Table A. 1 for a list of all abbreviations used) which then triggered the development of non-classical nucleation pathways and proposed the existence of prenucleation clusters (PNCs) to explain more adequately crystal nucleation processes.[5] Although, one of the concerns in interpreting experimental data is often to determine if the observed clusters are indeed on-path to form the final nuclei that can grow. Therefore, pre/post steady state kinetics measurements are required to differentiate if the "intermediate" PNC is kinetically on- or off-path to a final product, as stated in[5] and references within their review.

Ionic crystals that form in natural or engineered aquatic conditions generally form at non-stoichiometric conditions, as ionic ratios in such solutions can deviate strongly form the lattice ratios. In nature, this is due to external controls on ion concentrations such as weathering rates, microbial or hydrothermal activity. For example for our model system barite, in the pore waters of mud volcanoes, a variation in stoichiometry (cation:anion) from 0.00007 to 120 was reported.[6] For our model system calcite, the stoichiometry in natural waters varies with a minimal range of six orders of magnitude, from $5 \cdot 10^{-4}$[7] to $2.9 \cdot 10^{+2}$.[8] In industrial processes, the potential variation in stoichiometry is due to mixing of cation-rich and anion-rich water.[9,10] This mixing causes mineral scale formation leading to technical problems e.g., suppression of the heat transfer efficiency in cooling systems and occlusion of the piping leading to a drastic increase of the operational costs as addressed in more detail in review papers like.[11,12] In these natural and industrial cases of deviating ionic ratios in solution, ionic crystals like our model systems, form under non-stoichiometric conditions.

Experimental work at non-stoichiometric conditions showed that the nucleation rate and initial growth differ, particles formed are charged due to excess lattice-ion adsorption and

[a] J. A. Koskamp, S. Y. M. H. Seepma, V. F. D. Peters, M. Wolthers
Department of Earth Sciences, Utrecht University, 3584 CB Utrecht, The Netherlands
Tel.: +31302535042
E-mail: j.a.koskamp@uu.nl
s.y.m.h.seepma@uu.nl
v.f.d.peters@uu.nl
m.wolthers@uu.nl

[b] D. Toroz, D. Di Tommaso
School of Physical and Chemical Sciences, Queen Mary University of London, Mile End Road, London, E1 4NS, UK
E-mail: d.toroz@qmul.ac.uk
d.ditommaso@qmul.ac.uk

Supporting information for this article is available on the WWW under https://doi.org/10.1002/chem.202303860

the nucleation and growth theories fall short.[13–20] Moreover, an asymmetrical behaviour was observed when studying the particle formation rate as a function of solution stoichiometry.[13] When there is an excess of one of the crystal-building ions, it is more likely that the initial steps of nucleation go through the formation of charged triple ion complexes (CTICs,[21]), rather than via ion pair aggregation (e.g.[11]). Such triple-ion complexes can be positively or negatively charged depending on the solution stoichiometry. CTIC have been simulated[22] and have been observed experimentally. More specifically, positive CTICs have been detected in several Raman and dielectric relaxation spectroscopy (DRS) experiments,[23–26] while negative CTICs are undetectable by DRS.[26] Both, positive and negative CTICs have been observed qualitatively using mass spectroscopy.[27] Possibly, these CTIC play a role in the change of nucleation kinetics with non-stoichiometric ratios of lattice ions. Note that, while CTICs have been observed under certain conditions, to the authors knowledge, there is currently no experimental evidence that CTICs function as intermediate species "on path" to nucleation of either barite or calcite formation. Previously, it has been found that the smallest complexes are the most affected by charge imbalance because of non-stoichiometry.[28] This was dedicated to the high repulsive force in a small cluster, whereas for larger complexes both the surrounding water and the increased bulk help stabilize the cluster, weakening the effect of charge imbalance.[28] This suggests that the effect of charge on the stability is predominantly observable in the small complexes. For this reason, we hypothesise that this impact of charge-imbalance in prenucleation clusters causes the reported asymmetry of nucleation (rate) with solution stoichiometry. We quantified differences in thermodynamic stability and life-time of the smallest possible complexes with charge imbalance – positively and negatively CTICs – for the two model mineral systems. To attribute our observations to either the cation or the anion we also crosslinked the ions. This meant that we studied the combinations of two cations (Ba^{2+} and Ca^{2+}) and two anions (CO_3^{2-} and SO_4^{2-}), resulting in the formation of CTIC related to barite, witherite ($BaCO_3$), calcite, and gypsum ($CaSO_4.2H_2O$). We obtained insights into the thermodynamic stability of the formation of these CTIC, by determining the association constants. Complementary, kinetic insights were obtained via differences in activation energy barriers, which dictate the minimum energy required for reactants (in this case CTICs) to transform into products. The related variation in lifetimes of CTICs represents differences in contributions to nucleation and subsequent growth.[29] Lifetime, also known as the dissociation time or relaxation time, quantifies the duration during which an ion pair or CTIC remains intact before dissociating into its constituent ions. A longer lifetime means a higher probability to grow further via the diffusion-limited addition of extra ions.[29] In this study, we obtained the configuration, stability and lifetime of the CTIC that form on-path to nucleation using classical molecular dynamics (MD) in combination with metadynamics. We also performed dynamic light scattering (DLS) experiments to study the evolution in particle size at the early stages of mineral formation. Differences in association constants and lifetime for the positively and negatively CTIC were observed in the simulations that could be related to the early trends observed experimentally during particle formation.

Methods

Computer Simulations Methods

Classical Molecular Dynamics. All molecular dynamics simulations in this study were performed using the LAMMPS code.[30] All simulations were performed at a temperature of 300 K and, during the 100 ps equilibration period in the NPT ensemble, the pressure was kept at 1 atm. The thermostat and barostat were taken from Nosé–Hoover[31,32] with 0.1 and 1 ps relaxation times, respectively. The equations of motion were integrated using the velocity-Verlet algorithm[31,32] with a time step of 1 fs. The simulation cells were cubic boxes with a length of ~32 Å containing 1105 SPC/Fw[33] water molecules, four ions of interest (Ba^{2+}, Ca^{2+}, CO_3^{2-}, and/or SO_4^{2-}) plus two background ions (Na^+ or Cl^-). For the positively charged triple ion complex (CTIC) formation, the anion was fixed in the middle of the box. The two cations were allowed to move freely to explore all metastable configurations, i.e., the solvent- separated ion pair (SSIP) describing a pair of single ions, solvent-shared ion pairs (SIP) and the contact ion pair (CIP). For the negatively CTIC formation, it was inversed, with the cation fixed in the centre of the cell. Two counter charged background ions were fixed in the corner of the box balancing the charge. The minimum distance between the two ions was >1.08 nm and the distance to the central ion >1.87 nm, considering periodic boundary conditions. The neutral ion pairs (IPs), $BaCO_3^0$, $BaSO_4^0$, $CaCO_3^0$, and $CaSO_4^0$, were simulated in water boxes of the same size to validate our method with published experimental and computational work. In this case the cation was fixed in the centre of the box and the anion was free to move.

Force field. The parameters for the water are those of the SPC/fw force field,[33] which we have chosen given the validated $CaCO_3$ interactions.[34,35] For the carbonate systems the Ca^{2+}, Ba^{2+} and CO_3^{2-} ions were simulated using the parameters from.[35] The parameters for the calcium sulfate system were taken from[36] in which they described SO_4^{2-} according to.[37] The $BaSO_4$ parameters were taken directly from,[37] using the sulfate-water$_{SPC/fw}$ from.[36]

Metadynamics. The free energy landscapes and profiles were calculated from well-tempered metadynamics simulations using the PLUMED 2.5.3[38] plug-in for LAMMPS. The collective variables (CVs) used were the distances between the central ion and both counter ions or the distance between the two ions with opposite charge for the CTIC and the neutral IP formation, respectively. Gaussian hills were deposited every 1 ps with a hill height of 1.0 kJ mol^{-1} and a width of 0.02 nm. The bias factor was set at 10. We explored the 2D free energy surface (FES) and 1D energy profiles up to a CV distance of 1.2 nm, since we were interested in the association mechanism and the formation of the smallest charged complex. We placed an upper wall at 1.6 nm with a force constant (κ) of 2000 on each CV. The total simulation time was 2.14 μs per metadynamics simulation to achieve convergence. Subsequently, the free energy profiles of the two CVs in the FES were extracted by integrating out one of the CVs resulting in a horizontal and vertical profile.

Calculation of association constant. The formation of the smallest charged complex can be described with two association constants. The first one is the association constant (K_a) for the formation of an ion pair, while the second association constants K_{a2+} and K_{a2-} are the constants for the association of the cation or anion with the overall neutral ion pair, respectively. The comparison between the

free energy profiles from the metadynamics simulations and the experimentally obtained association constant (K_a) was achieved through predicting the K_a from the free energy profiles as function of the cation-anion distance. K_a, K_{a2+} and K_{a2-} are stability constants, in the literature also referred to as the formation, association or binding constant, and are defined in terms of activities as:

$$K_{a1} = \frac{a_{AC}}{a_A a_C},\ K_{a2+} = \frac{a_{ACC^+}}{a_{AC} a_C},\ K_{a2-} = \frac{a_{AAC^-}}{a_{AC} a_A} \tag{1}$$

where a_{AC} is the activity of the anion (ligand)-cation complex, while a_A and a_C are the activities of the free anions and cations in solution. The activity of the charged complexes is given by a_{ACC} and a_{AAC}, positively and negatively charged, respectively. In an infinitely dilute solution, all activity coefficients (γ) are equal to one and another way of expressing K_a^{∞} is:[39]

$$K_a^{\infty} = \frac{[Complex]c^{\ominus}}{[Receptor][Ligand]} = c^{\ominus} a_{\ominus} \int_0^{R_U} e^{-\frac{\Delta G(r)}{k_b T}} dr \tag{2}$$

with $c^{\ominus}$ as the standard state concentration (6.022×10^{26} molecules per m^3), $a_{\ominus}$ is a reference surface which was set as $10^{-20}\ m^2$ representing the typical order of magnitude studied with MD. $\Delta G(r)$ is the free energy in J as a function of the CV distance, k_b the Boltzmann constant (J/K) and T the temperature in K. The radial distance (r) in meter and R_U correspond to the maximum distance of the associated state and is set at 1 nm for all systems to include all metastable association structures until the CIP.[40] However, the choice of R_U is only weakly affecting the actual value of the association constant.[41] The $\Delta G(r)$ was determined from the radial distribution function (RDF) of the cation and the anion, $g^{id}(r)$ by using statistical mechanics:[39]

$$\Delta G(r) = -k_b T \ln\left(4\pi r^2 a_{\ominus}^{-1} g^{id}(r)\right) \tag{3}$$

The free energy profile was aligned with the analytical solution of a screened electrostatic potential, keeping in mind the impact of the ionic strength on the Debye length and dielectric constant. This analytical solution of the free energy as a function of distance (r) was given by:[39]

$$\Delta G(r) = \frac{1}{4\pi\varepsilon_0} \frac{q_i q_j}{\varepsilon_r(c) r} e^{-r/\lambda_D} - k_b T \ln\left(4\pi r^2 a_{\ominus}^{-1}\right) \tag{4}$$

where q is the electric charge of the particles i and j in coulomb, ε_0 is the permittivity in vacuum, $\varepsilon_r(c)$ water dielectric constant as a function of the electrolyte concentration (c) in mol/L, and λ_D is the Debye length in meter:[39]

$$\varepsilon_r(c) = \varepsilon(0) - (\varepsilon(0) - \varepsilon_{ms}) L\left(\frac{3\alpha}{(\varepsilon(0) - \varepsilon_{ms})} c\right) \tag{5}$$

where $\varepsilon(0) = \varepsilon_{SPC/fw}$ which is 78.1 at 298.15 K.[42] ε_{ms} is the limiting dielectric constant of the highly concentrated electrolyte solution, in other words, the molten salt dielectric and was set at 30.08.[43] The Langevin function is written as $L(x) = \coth(x) - 1/x$. The total excess polarization parameter in L/mol,[43] α, was estimated for the positive and negative complex at 28.5 and 26.0, respectively, based on the experimental values[44] for Na^+, Cl^-, Ba^{2+} and SO_4^{2-}. The values for Ca^{2+} and CO_3^{2-} were missing, however we approximated them to be similar to Ba^{2+} and SO_4^{2-}, respectively, and therefore used the same values. Using the value Mg^{2+} instead of Ba^{2+}, resulted in insignificant changes of ~0.0009 kJ/mol in association free energy. The importance of the consideration of the electrolyte concentration in the dielectric constant and therefore in the analytical solution of the free energy, could be observed in Figure 1, where one expects the profiles obtained from MD to be converged with the analytical solution after 0.9 nm (the cut off distance of the short-range interaction in the used forcefield). As could be seen, when there is no correction for the ionic strength (IS), the two lines were divergent Figure 1. This was improved after considering the electrolyte concentration in the analytical solution, however a smaller divergence remained. The most probable explanation for this observation is that we explored the energy surface where both counterions are within a radius of 1.2 nm from the central (cat)ion, due to our metadynamics simulation set up. As a result, the local electrolyte concentration in this spherical volume was much higher than the overall electrolyte concentration of the whole water box. Considering this higher concentration, we were able to align the tail (>0.9 nm) of the free energy profile with the tail of the analytical solution.

The obtained K_a represents the ratio between complex and the reactants assuming all activity coefficient (γ) to be equal to unity. This is only true in pure water or infinitely diluted solutions. There are several theories that can be used to estimate the γ, depending on the concentration one can use a less or more advanced theory. While the Debye-Hückel theory is accurate for low IS (<0.1 M),[45] Pitzer's model is more applicable for high concentrations as the model considers charge, average size, binary and ternary interactions, and distinguishes between ions of opposite and same sign.[45] In this study we have a low background electrolyte concentration of 0.0996 M and we therefore could have opted for the Debye-Hückel theory. We used the extended Debye-Hückel theory,[46] since we had ions and charged complexes of different sizes:

$$\log_{10}\gamma_i^{EDH} = -A z_i^2 \frac{\sqrt{IS}}{1 + B a_i \sqrt{IS}} \tag{6}$$

where $A = -1.824928 \times 10^6 (\varepsilon_r T)^{-3/2}$, $B = 50.3 \times 10^6 (\varepsilon_r T)^{-1/2}$, z_i was the charge number of ion species i, the term a_i was the effective diameter of the hydrated ion in angstroms. For the single ions we used the rounded values based on the ionic mobilities.[46] The diameter for the charged triple complexes is not straightforward to estimate, we therefore chose to estimate a maximum and minimum diameter. The maximum diameter was calculated from the sum of the volumes of the individual ions using their individual a_i. And the minimum diameter was taken from the ion with lowest value for a_i. The average, upper and lower value were used to indicate the deviation on the association constants.

The activity coefficients of the neutral ion pairs generally follow the empirical Setschenow equation ($\gamma = \ln(K_s C_s)$[47]) and is usually set at 1 since the K_s is assumed to be small and approached to zero.[45] However, studies have shown that K_s might not be insignificant[48,49] and can be estimated using:[50]

$$K_s = \frac{V_{intr} \times \left(V_{intr} - V^{\circ}\right)}{\kappa_T RT} \tag{7}$$

where V_{intr} is the intrinsic volume calculated as the sum of the partial molal volumes of the ions in water[51] and the individual ionic volumes, V°.[52] κ_T is the isothermal compressibility of the solvent and was 0.457 GPa^{-1} in this case water[53] and R is the gas constant.

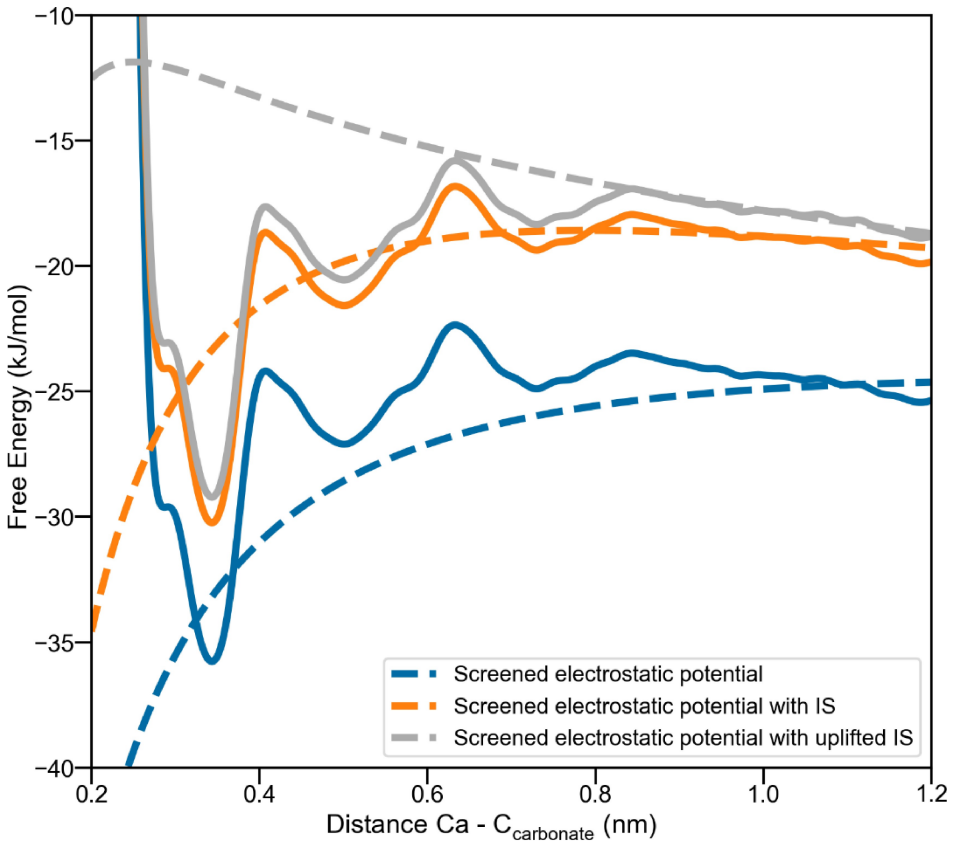

Figure 1. Energy profiles of $CO_3 - -CaCO_3$ pairing aligned with three different analytical solutions of the screened potential using equation 4 (dashed lines). The analytical solution without considering the effect of the ionic strength (blue line), considering the overall ionic strength (orange line) and considering the uplifted ionic strength by the CO_3 present in the CIP configuration with Ca upon the association of an extra CO_3 (grey line).

The final association constant for the charged triple ion complexes was then obtained by multiplying the association constant assuming infinite dilution, K_a^{∞}, calculated using equation 2, with the activity coefficient term:

$$K_{a2+} = \frac{\gamma^{EDH}_{ACC^+}}{\gamma^{Setschenow}_{AC}\gamma^{EDH}_{C}} K^{\infty}_{a2+}, \quad K_{a2-} = \frac{\gamma^{EDH}_{AAC^-}}{\gamma^{Setschenow}_{AC}\gamma^{EDH}_{A}} K^{\infty}_{a2-} \tag{8}$$

This standard association constant was converted into the Gibbs free energy of association (ΔG_a) in kJ/mol:

$$\Delta G_a = -RT\ln(K_a) \tag{9}$$

Calculation of lifetime. The lifetime of the charged complexes can be computed by the inverse of the rate constant (k_d). Using the free energy of activation ($\Delta G^{\dagger}$), the transition state theory provides a method to calculate the rate constant:

$$k_d = A' e^{-\Delta G^{\dagger}/RT} \tag{10}$$

where A' is a pre-factor with unit s^{-1}, T is the temperature in K, and R is the gas constant (8.314 J mol/K). The pre-factor, $A' = \kappa k_b T/h$, was deliberately used to distinguish from the pre-exponential A factor in the classic Arrhenius equation and describes the frequency at which a system oscillates in its minima, and the exponential factor describes the probability to cross the activation energy. There are several ways to calculate A',[54] the one we used in this work was by determining the second derivative at the minimum of the well (E'') and relating it to A' by $A' = 1/2\pi\left(E''/\mu\right)^{1/2}$, where μ is the reduced mass of the ion pair. The E'' was obtained by fitting a polynomial of the second order to ten data points centred around the minimum of the well.[54] The standard deviation (SD) was calculated from the horizontal and vertical free energy profile in the case of the CTIC. For the neutral ion pairs, the SD was calculated from the last 31 ns. For A', the SD was derived from the covariance matrix of the polynomial fit. The corrected sample standard deviation was used for the SD of $\Delta G^{\dagger}$. The propagation of the SD was done by keeping in mind the equations for propagating uncertainties for the mathematical functions.

Experimental Methods

Growth solutions. In this study we used the same method, to study $BaSO_4$ at non-stoichiometric conditions,[14] for $CaCO_3$. In short, we employed Visual MINTEQ, a free equilibrium speciation model version 3.1,[55] to define three distinct growth solutions. These solutions were differentiated by their {cation}:{anion} ratio, with one solution being stoichiometric (with a r_{aq} of 1), and the other two being non-stoichiometric, with either an excess of anions (r_{aq} approximately 0.01) or an excess of cations (r_{aq} approximately 100). The initial degree of supersaturation (Ω) was constant for all systems, and was determined relative to the most thermodynamically stable solid phase by dividing the ion activity product (IAP) by the solubility product (K_{sp}). The -log(K_{sp}) values for $CaCO_3$, was established as 8.48.[56] Reagent-grade salts of $CaCl_2$, Na_2CO_3, and NaCl (Merck; 99.5% purity) were dissolved in Milli-Q water (i.e. ISO 3696 Standard Grade 1–18 mΩ) to produce stock solutions with

varying concentrations. These stock solutions were utilized to create growth solutions, each comprising 250 mL of solution, which were stored in capped bottles (Greiner) with limited headspace. The growth solutions were used for DLS experiments within a 48-hour period to minimize CO_2 dissolution.[57] The ionic strength of the solutions was adjusted by addition of NaCl (Sigma-Aldrich). The targeted ionic strength (IS) for the experiments was set at 0.34 M to align with the MD simulations. The Davies equation,[58] which is valid for IS $\leq$ 0.5 M, was utilized to calculate the ion activities. The computations in Visual MINTEQ were performed at a temperature of 27 °C, which was the average temperature during the experiments, and under a closed atmosphere. The growth solutions and their corresponding physicochemical parameter values are listed in Table 1. The desired pH for the growth solutions was set at 11 to minimize the effect of bicarbonate in $CaCO_3$ formation.

Dynamic light scattering. The nucleation of the minerals in stoichiometric and non-stoichiometric ratios was studied using dynamic light scattering (DLS) in flow with the Zetasizer ULTRA, equipped with ZS XPLORER v1.2.0.91 software[59] and an Ismatec IPC series peristaltic pump using flow tubing with 1.52 mm internal diameter. The experiments were performed in backscattering detection angle. We used a wavelength of 632.8 nm.[13] All DLS measurements were conducted at a temperature of 27 $\pm$ 0.1 °C for the growth solutions (Table 1). The particle sizes were calculated using the non-negative least squares as the discrete inversion approach[60] in combination with a regularization method, called Multiple Narrow Modes. This method has a high chance of observing multiple particle size populations during nucleation and growth (e.g.[14]). The Multiple Narrow Modes approach uses quadratic weighing of the correlation data, has the regularizer fixed to 0.001 and uses 70 fixed size classes.[13,61] For the experiments with $CaCO_3$, we initially used a flow rate of 8 ml/min for $\Omega_{calcite}$ = 100 to be consistent with earlier work[13] and the barite measurements in terms of particle densities. A flowrate of 8 ml/min was preferred to prevent scale formation in the tubing before the DLS flow cell. For $\Omega_{calcite}$ = 70, further optimalisation was needed to observe differences in particle formation at different stoichiometric ratios. This was obtained a lower flow rate of 2 ml/min, likely (also) because $CaCO_3$ (ACC/vaterite/calcite) particles are better approximated by a sphere compared to tabular $BaSO_4$ particles.[13,17,62] Therefore, $CaCO_3$ particles, migrate faster through the solution compared to $BaSO_4$ particles.[63] Consequently, it was more difficult to detect low particle concentrations of $CaCO_3$, since insufficient particles stayed within the measurement scattering volume within a subrun. This is in line with the observations for spherical silica nanoparticles of 50 nm when a flow rate of 8 ml/min was used (Figure S28-j).

The measurement process included 20 subruns of 1.68 s, with a constant flow rate resulting in a fixed time within the process of nucleation and growth. Each measurement was repeated for at least 5 times. The temperature equilibration time was set to 10 s. More details on the methodology, pump settings and tubing used during the DLS flow experiments were reported in.[13] We cleaned the sample cell and tubing with 0.2 mol/L HCl before flushing it with Milli-Qwater before starting the next experiment. For comparison of our DLS and simulation results, it is noteworthy that for $BaSO_4$, barite particles with a typical size of 10 nm contain approximately ~6000 ion pairs, while in our MD simulations the clusters contained only a few ions. For $CaCO_3$, calcite particles of 10 nm contain ~8500 ion pairs, while a 1000 nm particle contains ~8.5 billion ion pairs, keeping in mind that the number of ion pairs in a $CaCO_3$ particle depends on the polymorphs that form.[64]

Results

Computer Simulation Results

Free energy surfaces of charged triple ion complex formation. The free energy surfaces (FESs) obtained using metadynamics varied with ionic-ratio of the CTIC for all systems investigated (Figure 2). An example of a free energy surface in the 3 dimensional space of energy versus distances between ion-pairs and third ions is shown in Figure 2-I. This figure illustrates the shape of the wells, hills, and trenches (for a 3D representation of all systems see SI Figure S1). The intensity plots in Figure 2-II display the pairing free energy as a function of the same ion distances. In these figures, the 3rd dimension of free energy is indicated by colours, with brighter yellow colours indicating higher energy and darker purple colours representing lower energy. The FES analysis revealed multiple wells and energy barriers. Deeper energy wells indicated more energetically favourable configurations. For almost all studied systems, the contact ion pair (CIP, Figure 3) configuration was observed in four distinct wells at ion distances below 0.4 nm. These wells corresponded to combinations of mono and bidentate coordination, Figure 2. The bi-biCIP configuration (both ions in bidentate CIP configuration with the central ion, Figure 3a) was found at ~0.32 nm, while the mono-monoCIP configuration (i.e. both ions in a monodentate CIP configuration with the central ion, Figure 3b) occurred at ~0.40 nm. Combinations of mono and bidentate configurations (mono-biCIP) were also observed (Figure 3). Wells at around 0.5 nm represented the solvent shared ion pair (SIP, Figure 3c). At the boundary between association and dissociation, a well at approximately 0.75 nm

Table 1. Chemical properties of the growth solutions for $CaCO_3$.

[Cation] (μmol/L)	*[Anion]*	a_{cation}	a_{anion}	$IS_{initial}$ (mol/L)	$pH_{initial}$	Ω	r_{aq}	*flowrate* mL/min
755	54200	57	5685	0.3399	11.006	100.2	0.01	8
3010	6010	569	568	0.3403	11.002	100.2	1.00	8
25300	1010	5686	57	0.3411	11.003	100.2	100	8
563	46350	47	4861	0.3376	10.995	70.8	0.01	2
2453	5000	476	479	0.3394	11.005	70.8	1.00	2
21200	788	4775	48	0.3400	11.005	70.8	100	2

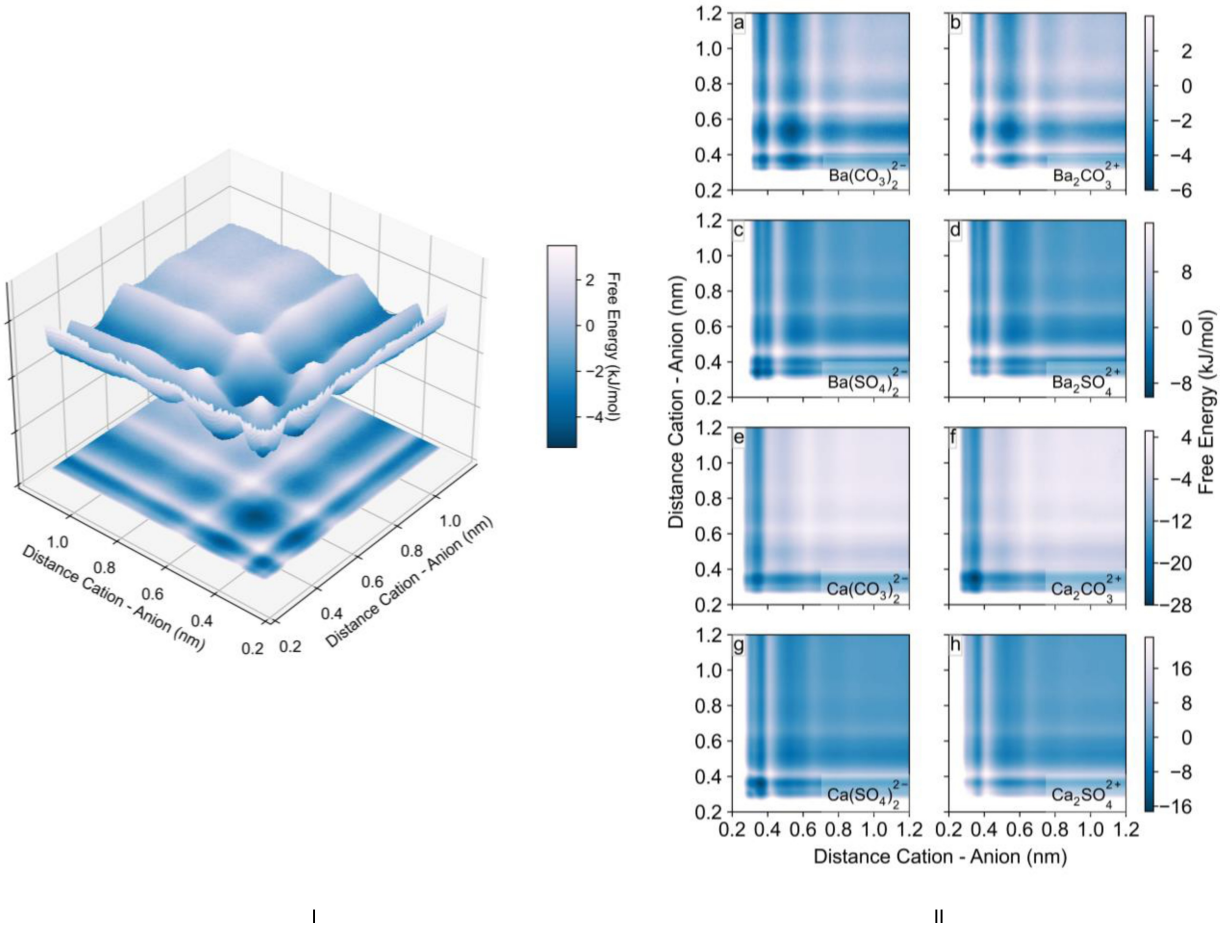

Figure 2. I) Illustrative 3D representation of a free energy surface of CTIC with a 2D projection of the surface at the bottom of the graph that is identical to IIa. II) Free energy surfaces of negatively and positively charged complex formation as a function of the distances between the central ion and either counter ion, respectively on the x and y axis at 300 K in aqueous solution. With a) $Ba(CO_3)_2^{2-}$, b) $Ba_2CO_3^{2+}$, c) $Ba(SO_4)_2^{2-}$, d) $Ba_2SO_4^{2+}$, e) $Ca(CO_3)_2^{2-}$, f) $Ca_2CO_3^{2+}$, g) $Ca(SO_4)_2^{2-}$, and h) $Ca_2SO_4^{2+}$.

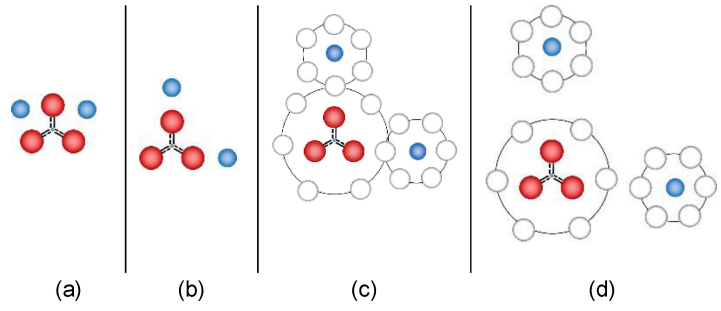

Figure 3. Schematic representation of example CTIC configurations of calcium carbonate, with Ca^{2+} (blue), CO_3^{2-} (red), and water (white): (a) bidentate contact ion pair (bi-biCIP), (b) monodentate contact ion pair (mono-monoCIP), (c) solvent-shared ion pair (SIP), and (d) solvent-separated ion pair (SSIP).

corresponded to the solvent separated ion pair (SSIP, Figure 3d).

For the various cation-anion systems and non-stoichiometries, different types of ion pair configurations were found to be the most stable species in solution. For the barium sulfate system (Figure 2c and d), a bi-biCIP with excess sulfate was overall the most stable complex, also compared to any barium-excess complex. Among the excess barium CTIC, a SIP configuration was most stable and the mono-monoCIP was more stable than the bi-biCIP. For calcium carbonate complexes (Figure 2e and f), a mono-monoCIP was the most stable configuration for cation and anion excess systems, with the excess calcium CTIC as the most stable, implicating that the positive CTIC was more stable than the negative CTIC. For the crosslinked systems, barium carbonate and calcium sulfate, SIP complexes were the most stable for all systems except for those with excess calcium, Figure 2a, b, g and h. The complexes with excess anion were more stable than excess cation complexes.

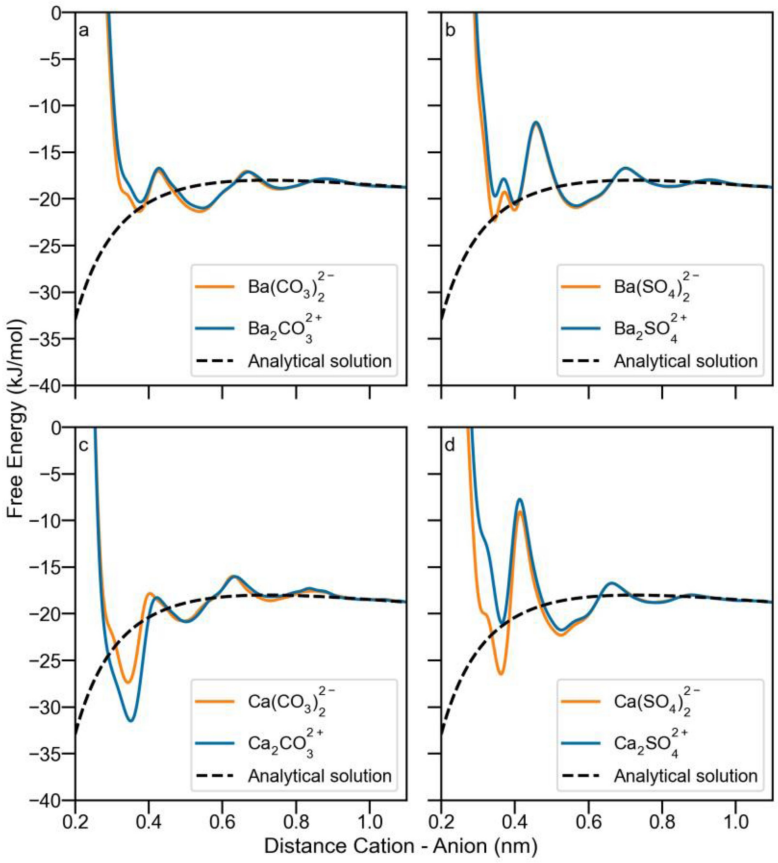

Figure 4. Energy profiles of the positively (blue) and negatively (orange) CTIC formation aligned with their respective analytical solution of equation 4 solutions of the screened potential using equation 4 (dashed lines) at 300 K in water; for $BaCO_3$ (a), $BaSO_4$ (b), $CaCO_3$ (c), and $CaSO_4$ (d).

The wells and barriers in the FESs of the systems with calcium were deeper and higher compared to the systems with barium.

Association constant and association free energy of charged triple ion complexes. The association free energy profiles for addition of the third anion (e.g., $CaCO_3 + CO_3^{2-} \rightarrow Ca(CO_3)_2^{2-}$) or cation (e.g., $CaCO_3 + Ca^{2+} \rightarrow Ca_2CO_3^{2+}$) to the neutral CIP (Figure 4), obtained from the FES, depend on non-stoichiometry. All energy profiles are aligned with the analytical solution as described in section Methods. The association constants corrected for the ion activities (K_{a2+} or K_{a2-}) and association free energies (Table 2) were calculated as the average of the horizontal and vertical free energy profiles ([22] Figure 4). The association constants and free energies without correction can be found in the supplementary information Table S1. For the barium systems, CTIC showed very comparable association free energies, while for the calcium systems the CTIC showed more variability. The $BaCO_3$ and $BaSO_4$ systems showed a slightly higher free energy for the negative complexes. However, due to the higher uncertainties in the estimation of the complex volumes, this difference was within the estimated error hence the positive and negative triple ion complexes were indistinguishable in terms of association energy. For the calcium sulfate complexes, the negatively CTIC was also more stable by 1.2 kJ/mol than the positively CTIC (Table 2). Contrastingly, for $CaCO_3$ the positive complex was the most stable, yielding a K_{a2+} of 81 ± 17, which is the largest association constant of all triple ion complexes studied (Table 2). The negative complex had a K_{a2-} of 22 ± 2, resulting in a difference of $-\Delta G_{a2+/-}$ of 3.3 kJ/mol.

Table 2. Calculated thermodynamic data using equation 8 and 9 in the Methods Section, at 300 K, and for aqueous solution for charged complexes; the association constants ($K_{a2+/-}$) and its free energy ($-\Delta G_{a2+/-}$) of charged triple ion complexes. The indicated error was the propagation of the error in K_a^{∞} which was taken as mean deviation from the mean, and the estimated deviation in the activity coefficients.

System	$K_{a2+/-}$	$-\Delta G_{a2+/-}$ *(kJ/mol)*
$Ba_2CO_3^{2+}$	9.2 ± 0.8	5.5 ± 0.2
$Ba(CO_3)_2^{2-}$	10.3 ± 1.2	5.8 ± 0.3
$Ba_2SO_4^{2+}$	9.3 ± 1.0	5.6 ± 0.2
$Ba(SO_4)_2^{2-}$	10.6 ± 1.1	5.9 ± 0.2
$Ca_2CO_3^{2+}$	81 ± 17	11.0 ± 0.5
$Ca(CO_3)_2^{2-}$	22 ± 2	7.7 ± 0.2
$Ca_2SO_4^{2+}$	10.4 ± 1.5	5.8 ± 0.3
$Ca(SO_4)_2^{2-}$	17 ± 2	7.0 ± 0.2

Kinetics of charged triple ion complex. The energy barriers for association, $\Delta G_a^{\dagger}$, and dissociation, $\Delta G_d^{\dagger}$, were determined as the association/dissociation of an extra ion to/ from a neutral IP which is constrained in a CIP configuration. The $\Delta G_d^{\dagger}$ for $BaSO_4$

was higher for the negative than the positive complex (Table 3 and SI Figure S2), while the $\Delta G_d^\dagger$ for $CaCO_3$ was higher for the positive than the negative complex (Table 3 and SI Figure S2). For the crosslinked systems, the $\Delta G_a^\dagger$ configuration was lower for the negative than the positive complex (Table S2). Conversely, the $\Delta G_d^\dagger$ was lower for the positive complex (Table 3 and Figure S2).

The CIP-CIP lifetime of the charged complexes was calculated from the energy profiles using equation 10, which relates the $\Delta G_d^\dagger$ to the rate constant of dissociation, k_d, according to equation 10. As shown in Table 3, the lifetime of charged complexes varies from 24 ps to 17 ns. The differences between the positive and negative complexes were more pronounced for Ca^{2+} than for Ba^{2+}. For barium, the lifetimes for the positively and negatively CTIC were in the same order of magnitude, although slightly longer lifetimes were observed for the negative complexes. For calcium, contrastingly, the $Ca_2CO_3^{2+}$ CTIC showed six times longer lifetime than the $Ca(CO_3)_2^{2-}$, compared to a 48 times longer lifetime for the negative calcium disulfate CTIC.

Free energy profiles, association constants, and kinetics of neutral ion pairs. A direct comparison of the thermodynamic and kinetic data between the CTIC and the neutral IPs is not possible since the neutral IP is part of the CTIC. Nevertheless, the most stable configuration for all CO_3^{2-} systems was the mono-CIP for both cations, Figure 5. For the ion pairs with SO_4^{2-}, the profiles show less strong variation for distinct configurations. Still, for $BaSO_4^0$ the bi-CIP configuration was more stable while for $CaSO_4^0$, the mono-CIP and SIP showed comparable stability (Figure 5).

Upon association, the CO_3 systems had to overcome a smaller $\Delta G_a^\dagger$ compared to the SO_4 systems, specifically, 3.88 kJ/mol for $BaCO_3^0$ and 1.86 kJ/mol for $CaCO_3^0$ compared to 8.45 kJ/mol for $BaSO_4^0$ and 13.26 kJ/mol for $CaSO_4^0$ (SI Table S3). The energy barrier for the system to overcome to dissociate the ions follows a different trend (SI Table S3). In this case we observed a higher energy barrier for the Ca systems, with a $\Delta G_d^\dagger$ of 14.49 kJ/mol for $CaCO_3^0$ and 13.07 kJ/mol for $CaSO_4^0$. The Ba containing systems had a $\Delta G_d^\dagger$ of 4.8 kJ/mol and 8.96 kJ/mol for CO_3 and SO_4, respectively. Table 4 shows the K_a^∞ and corresponding $-\Delta G_a$ based on the energy profiles in Figure 5. Note

Table 3. Kinetic data for charged complexes from the transformation of a CIP-CIP complex to a CIP-SIP complex and neutral IP going from CIP to SIP at 300 K and in aqueous solution; with pre-factor, A', the activation free energy of dissociation, $\Delta G_d^\dagger$, and the dissociation rate constant, k_d, (equation 10). Note that the values between brackets for the $BaCO_3$ system represent the transformation from SIP-CIP to SSIP-CIP complex and the neutral IP going from SIP to SSIP.

Complex composition CTIC	A' ($\times 10^9$ s^{-1})	$\Delta G_d^\dagger$ (kJ/mol)	k_d ($\times 10^9$ s^{-1})	Lifetime (ns)
$Ba_2CO_3^{2+}$	140 ± 8 (77.5 ± 2)	3.1 ± 0.4 (3.6 ± 0.3)	41 ± 7 (18 ± 2)	0.024 ± 0.004 (0.055 ± 0.006)
$Ba(CO_3)_2^{2-}$	180 ± 5 (94 ± 7)	4.03 ± 0.09 (4.0 ± 0.2)	35.8 ± 1.7 (19 ± 2)	0.028 ± 0.001 (0.053 ± 0.006)
$Ba_2SO_4^{2+}$	189 ± 3	8.4 ± 0.1	6.6 ± 0.3	0.151 ± 0.008
$Ba(SO_4)_2^{2-}$	207 ± 4	10.8 ± 0.03	2.68 ± 0.06	0.373 ± 0.008
$Ca_2CO_3^{2+}$	315 ± 8	13.2 ± 0.3	1.6 ± 0.2	0.64 ± 0.09
$Ca(CO_3)_2^{2-}$	241 ± 3	8.11 ± 0.05	9.3 ± 0.2	0.107 ± 0.003
$Ca_2SO_4^{2+}$	423 ± 14	12.5 ± 0.7	2.8 ± 0.8	0.3 ± 0.1
$Ca(SO_4)_2^{2-}$	303.0 ± 1.6	21.4 ± 0.7	0.058 ± 0.016	17 ± 5
Neutral IP				
$BaCO_3^0$	184.1 ± 1.1 (88 ± 3.3)	4.47 ± 0.06 (4.8 ± 0.10)	30.7 ± 0.7 (12.9 ± 0.7)	0.033 ± 0.0007 (0.078 ± 0.004)
$BaSO_4^0$	209.9 ± 0.5	8.96 ± 0.04	5.8 ± 0.1	0.173 ± 0.003
$CaCO_3^0$	352.2 ± 0.8	14.49 ± 0.08	1.06 ± 0.04	0.95 ± 0.03
$CaSO_4^0$	416.8 ± 1.0	13.1 ± 0.2	2.21 ± 0.17	0.45 ± 0.04

Table 4. Association constants for the neutral ion pairs at 300 K and in aqueous solution using equation 2, assuming infinite dilution (K_a^∞) with the corresponding association free energies ($-\Delta G_a$) using equation 9 compared to the range of values reported in literature.

System	K_a^∞	$-\Delta G_a$ *(kJ/mol)*	*Literature*	
			K_a^∞	$-\Delta G_a$ (kJ/mol)
$BaCO_3^0$	245 ± 5	13.72 ± 0.06	513[a]–6026[b]	15.56[a]–21.71[b]
$BaSO_4^0$	177 ± 5	12.92 ± 0.07	145[c]–533[c]	12.41[c]–15.66[c]
			20[d*]	7.47[d*]
$CaCO_3^0$	12024 ± 1067	23.4 ± 0.3	1660[e]–30409[e]	18.49[e]–25.75[e]
			1028[f*]–10106 [g*]	17.3[f*]–23.0[g*]
$CaSO_4^0$	173 ± 5	12.86 ± 0.08	141[h]–204[i]	12.35[h]–13.27[i]

The literature values are taken from: a,[65] b,[66] c,[67,68] d,[28] e,[56] f,[22] g,[69] h,[70] i.[71] The values with * were based on MD simulations.

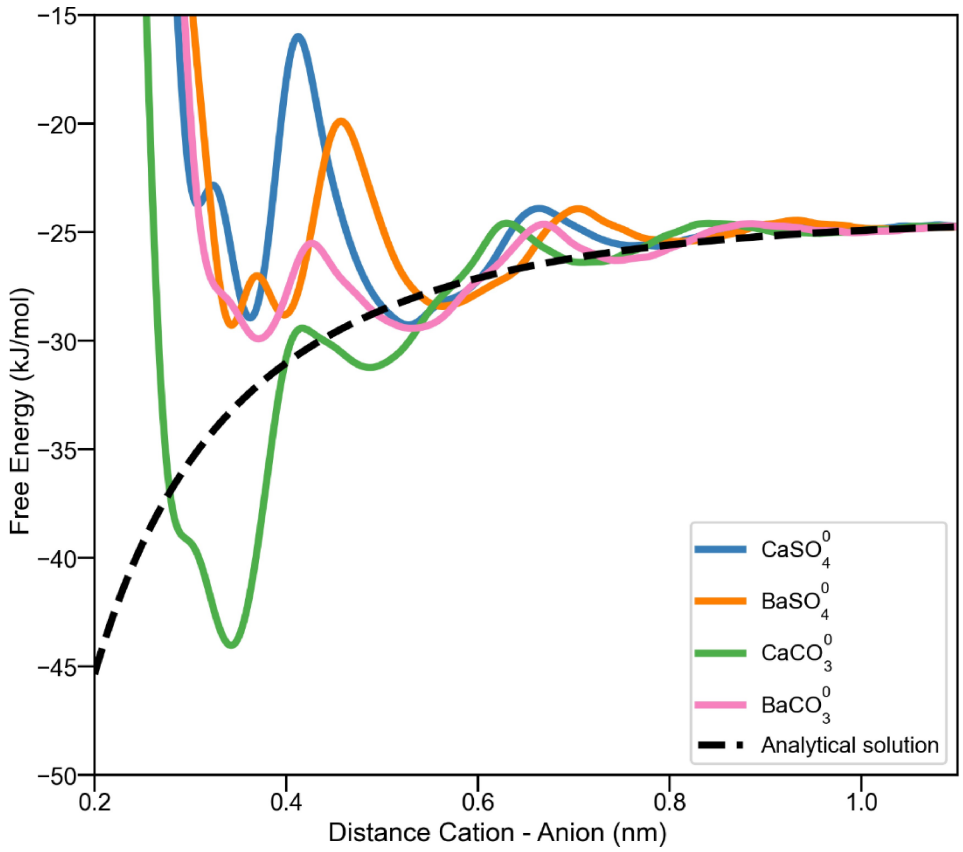

Figure 5. Energy profiles of the neutral ion pair formation aligned with analytical solution (dashed lines) at 300 K in water; for $BaCO_3^0$ (pink), $CaCO_3^0$ (green), $BaSO_4^0$ (orange), and $CaSO_4^0$ (blue).

that we did not need to correct these association constants for ionic strength effects of the solution, because the neutral IP systems were simulated in pure water assuming infinite dilution and ideal behaviour (i.e. activities are equal to concentrations). For the systems with sulfate, the difference in the K_a^∞ with Ba or Ca were indistinguishable. In contrast, for the carbonate systems, the K_a^∞ with Ca was approximately 50 times higher than Ba. All values were higher than the association constants found for the charged complexes (Table 2). In terms of lifetime, an interesting observation is that the $BaSO_4^0$ had a longer lifetime than $BaCO_3^0$, while $CaSO_4^0$ had a shorter lifetime than $CaCO_3^0$. This contrasts the general trend for most charged complexes where sulfates had longer lifetimes than carbonates. The lifetime of neutral ion pairs with sulfate was always between that of the positive and negative complexes, while the lifetime for the neutral ion pairs with carbonate was always longer than that of both charged complexes.

Evaluation of the collective variable and convergence. The distance between the central ion and the free counterions is an accepted collective variable (CV) to study association mechanisms.[22] We confirmed that this CV was also applicable to our systems as we observed that all profiles were smooth and without spikes (Figure 4).[72] In the intensity plots (e.g., Figure 2a and b), the free energy was plotted as a function of both distances. Convergence was achieved and evaluated by extracting and overlaying the horizontal and vertical profiles, as they both describe the change in distance for one of the counter ions from the fixed ion pair (see SI from Figure S3 to Figure S6). Additionally, the convergence was evaluated by comparing the energy profiles in time and their corresponding ΔG_{ass}; no significant changes were observed (see SI Figure S7 to Figure S11 for the CTIC and Figure S12 to Figure S16 for the neutral IP).

Experimental Results

Dynamic light scattering. To investigate the impact of solution stoichiometry on the initial stages of crystal nucleation, DLS experiments were carried out with a temporal resolution of less than one minute. The experiments were performed at stoichiometries (r_{aq} = the initial ratio of the free cation activity over the free anion activity) of 0.01, 1 and 100 and constant initial degree of supersaturation (Ω) and pH (see Table 1 for all experimental conditions).

For each system, the relative particle size information was acquired at 4, 10, 30, and 60 seconds after mixing the growth solutions and with a flow of 8 ml/min. The DLS results for the first timestep are reported in Figure 6a–f, while results for the longer mixing times and additional information on autocorrelation functions, diffusion coefficient distributions, and the

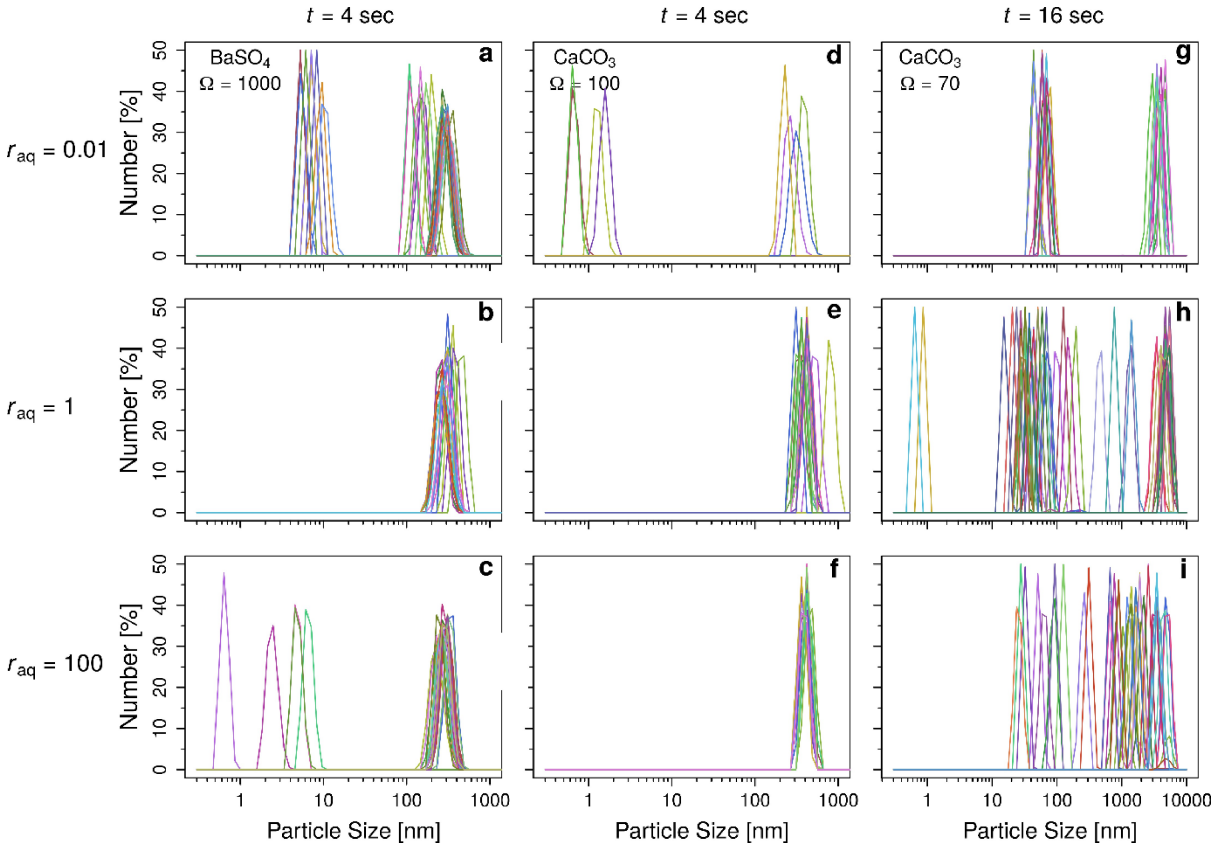

Figure 6. Particle size distributions for different solution stoichiometry for $BaSO_4$ ($\Omega_{barite} = 1000$) and $CaCO_3$ ($\Omega_{calcite} = 100$) mineral systems 4 seconds after mixing and with a flow rate 8 ml/min. The particle size number distributions are shown for $BaSO_4$: $r_{aq} = 0.01$ (a), $r_{aq} = 1$ (b), $r_{aq} > 100$ (c); for $CaCO_3$: $r_{aq} = 0.01$ (d), $r_{aq} = 1$ (e), $r_{aq} > 100$ (f). And for $CaCO_3$ ($\Omega_{calcite} = 70$) 16 seconds after mixing at a flow rate of 2 ml/min: $r_{aq} = 0.01$ (d), $r_{aq} = 1$ (e), $r_{aq} > 100$ (f). The different colours indicate the individual measurements. Note that the data for $BaSO_4$ is taken from[13] under the creative commons license.

intensity particle size distributions can be found in SI section 4 (Figure S17–Figure S21).

For $BaSO_4$, results were previously presented and discussed by Seepma et al.[13] and we re-evaluated these results in light of flow-measurements on a dilution series of a standard suspension with 50-nm-sized silica particles (SI section 5). A consistent peak at ~300 nm was observed at all stoichiometries and timesteps (Figure 6a–c, see discussion of this peak in SI section 5). At stoichiometric conditions and 10 seconds after mixing, smaller particles of 1–20 nm were observed and this population remained persistent over time (Figure 6b). At excess sulfate, particles that formed within 4 seconds were regularly <20 nm (Figure 6a), while at excess barium conditions, particles were occasionally detected with sizes that remained <10 nm (Figure 6c). This stochastic, asymmetric trend was consistent at increased time after mixing.

New DLS flow measurement during $CaCO_3$ nucleation and growth, at initial $\Omega_{calcite} = 100$ and a flowrate of 8 ml/min also showed an asymmetrical dependency with solution stoichiometry (Figure 6d–f). Again, a peak at ~300 nm was observed at all stoichiometries and timesteps (see SI section 5). At carbonate-excess conditions and t = 4 seconds (Figure 6d), small particles were observed in the range of 0.5–2 nm. At increased time after mixing, the particles' size increased slightly to 1–5 nm (Figure S20). At stoichiometric and calcium-excess conditions, however, no particles smaller than 300 nm were observed (Figure 6e and f).

A similar asymmetry of particle size evolution with solution stoichiometry was also observed at an initial $\Omega_{calcite} = 70$ and a flow rate of 2 ml/min (Figure 6g–i, Figure S22–S25). At these flow-rates, we observed a persistent peak at 1000–4000 nm at each r_{aq} and timestep conditions (i.e. Figure 6g–i, but also see Figure S26–S29 in the SI). At $r_{aq} = 1$ and t = 16 seconds (i.e. Figure 6h), we observed the largest range in particle size, from about 10 to 1000 nm, besides some particles of ~1 nm. With time, the system evolved into a bimodal particle size distribution, with populations of 10–70 nm and 300–1000 nm (Figure S24g). The particle sizes observed at $r_{aq} = 100$ (Figure 6i) were very comparable to those at $r_{aq} = 1$, although no peaks were observed at <10 nm. Contrastingly, at $r_{aq} = 0.01$ (Figure 6g), only peaks were observed in the range of 10 −100 nm. In addition, at $r_{aq} = 100$, particles of 10–100 nm persisted more frequently for up to 4 minutes (Figure S24i-l) compared to $r_{aq} = 0.01$ (Figure S24a–d).

Discussion

Thermodynamics and kinetics of the charged triple ion complexes. The interplay between association constants and

lifetimes plays a crucial role in determining mechanisms and probabilities of complexation reactions and particle formation in non-stoichiometric ionic solutions.[73] For instance, when the association constant is high and the lifetime is long, ion pairs tend to be stable and have a propensity to form larger clusters. Conversely, if the association constant is low and the lifetime is short, lower numbers of ion pairs form that are also more likely to dissociate quickly, hindering the formation of larger clusters. In cases where the association constant is low and the lifetime of the CTIC is long, complexes can still form, albeit at lower concentrations. If the association constant is high but the CTIC lifetime is low, or if there is a high activation barrier for association, the growth process may take an indefinitely long time. As the lifetime of a single complex increases, the probability of counter-ions binding to the CTIC also increases. This leads to the growth of the initial complex until it reaches a critical size where the effect of charge imbalances become less due to the stronger bulk-like behaviour.[28] The lifetime becomes increasingly significant in nucleation and growth contributions at lower ion concentrations.[73] Conversely, the association constant plays a more substantial role in higher ion concentrations, where a higher quantity of CTIC compensates for shorter lifetimes.

In terms of thermodynamics, our results reveal a disparity in the association constant between positively and negatively CTICs: in all systems the negative complexes were more stable, except for $CaCO_3$, where the positive complex exhibited a higher association constant. The observation for $CaCO_3$ aligns with a previous computational study,[22] providing further support to the reliability of our findings. It is worth noting that cations and anions are generally solvated differently in water. These differences in the solvation shells contribute to the energy profiles obtained here and therefore to the association constants (and lifetimes) of the CTIC, elucidating (part of) the differences between positive and negative CTIC. It should also be acknowledged that the difference in free energy of the charged triple ion complexes ($-\Delta G_{a2+/-}$ in Table 2) is relatively minor for $BaSO_4$. This is in line with the prevailing assumption depicted by Jones et al. in Figure 10 in their work for $BaSO_4$,[28] where they assumed no difference in positively and negatively CTIC.

In terms of kinetics, differences in activation energies between positive and negative complexes are predominantly observed upon dissociation. This underscores the significance of comprehending the lifetime of the CTIC (CIP-CIP configuration) and its dissociation (i.e. into SIP-CIP configuration). Specifically, our focus was directed towards the dissociation from the mono-CIP configuration, i.e., where the contact ion pair was in the monodentate configuration. This configuration represents the rate-limiting step for most systems typically characterized by the highest activation energy.[74] Note that for $BaCO_3$, the highest activation energy and therefore rate limiting step upon dissociation was found for the transition from SIP to SSIP.

The difference in stability and lifetimes for the calcium versus barium systems can be explained by the dissimilar chemical properties, such as lower atomic weight and size as well as higher electronegativity of calcium. This finding is consistent with the observation that water molecules coordinated with Ca exhibit a lifetime approximately one order of magnitude longer than those coordinated with Ba.[75] Furthermore, we observed a consistent trend in association constant in relation to the anion variation. In particular, CO_3-complexes displayed higher association constants compared to SO_4-complexes. This distinction can be attributed to the differences in size/geometry, electron structures and electronegativities between carbonate and sulfate ions, which influence their bonding capabilities with metal cations. In the case of carbonate, the central carbon atom lacks d-orbitals for back-bonding with metal cations, resulting in more electron density on the oxygen atoms.[76] This contributes to carbonate exhibiting a more pronounced ionic character in the metal-oxyanion interaction when compared to sulfate.[76] Conversely, the tetrahedral structure of the sulfate ion facilitates more effective back-bonding between sulfur and metal cations, resulting in more covalent character within metal-sulfate complexes,[76] resulting in a weaker bond compared to metal-carbonate complexes and therefore a lower association constant (as for the neutral IP, in agreement with literature, Table 4). We did not observe a consistent trend in lifetime as the cation significantly impacts the results.

By studying the effect of stoichiometry on the first steps of nucleation by MD simulations coupled with DLS flow experiments, insights into the early stages of particle formation were obtained. For both systems, we observe with the DLS particles much larger than the critical nucleus size, meaning that growth processes (potentially including agglomeration) contribute to the DLS data. However, the stochasticity of the DLS observations suggests a significant influence of the nucleation process as this is stochastic by nature. Therefore, the trends obtained with stoichiometry in the MD simulations can be related to the trends observed using DLS.

In the case of $BaSO_4$, for $r_{aq}=1$ we observed a single peak (~300 nm) at 4 seconds and with time also smaller-sized particles (0.8–10 nm) appeared. It is possible that a decrease in Ω at increasing time after mixing caused slower continuous nucleation (c.f.[5,11]) and growth that lead to a higher probability to capture smaller-sized particles.[13] The instantly and initially formed particles at 4 seconds were possibly part of the peak at 300 nm (as observed with other techniques, TEM and DLS-batch[13]) or were deposited on the inside of the tubing as scale formation (as visually observed with lower flow-rates) or were already larger in size than the DLS upper detection limit (although such large particles were not observed with TEM[13]). The fact that at 4 seconds we observe smaller-sized particles for $r_{aq}\neq 1$, implies that the nucleation and growth is slower than $r_{aq}=1$. Additionally, nucleation rate varied asymmetrically with r_{aq}, where nucleation was slower at cation excess than anion excess.[13] The shorter lifetime and lower association constant for the positively CTIC of $BaSO_4$ are in line with this asymmetry observation, suggesting that the difference in stability and especially lifetime of the CTIC may be the reason for the asymmetrical dependency of barite nucleation rate on solution stoichiometry.

For the $CaCO_3$ systems at $\Omega_{calcite}=70$, the higher peak intensities and the more consistent observation of particles at each timestep for $r_{aq}=1$ compared to $r_{aq}\neq1$, suggest that generally more particles were formed at stoichiometric conditions. The variability in particle size observed for $r_{aq}=1$ at 16 seconds after mixing suggests high stochasticity, this indicates that these observations were nucleation dominated[20] which is by nature more stochastic than growth.[77–79] A similar stochastic behaviour of particle formation was observed at $r_{aq}=100$. For $r_{aq}=0.01$ at $\Omega_{calcite}=70$, larger particles were less frequently observed compared to $r_{aq}=100$ and smaller particles were less persistent over time (Figure S25). Although less conclusions can be drawn from the results of $\Omega_{calcite}=100$, due to the lack of smaller-sized particles, the observation that $r_{aq}=1$ and $r_{aq}=100$ show similar behaviour is consistent with $\Omega_{calcite}=70$. The decreasing number of particle observations (i.e. number of peaks) over time for all stoichiometries is likely a result of sedimentation of large particles in the sample cell, due to particle growth or scale formation. All in all, our results suggest a dependency of particle nucleation on r_{aq} at constant initial Ω. This observation aligns with the larger association constant and longer CTIC lifetime for $Ca_2CO_3^{2+}$ compared to $Ca(CO_3)_2^{2-}$, meaning that the route via cation addition is more favourable compared to anion addition.

In both, MD simulations and experiments, we observed an asymmetrical behaviour of the CTIC and an asymmetrical observations of larger clusters, respectively. From this similarity it may be inferred that, in non-stoichiometric solutions, CTIC pathways might be kinetically on-path and dominant intermediates towards critical nuclei. Additionally, aggregation of neutral ion pairs into larger PNC and nuclei is likely less dominant under non-stoichiometric conditions. It is therefore important to consider non-stoichiometry, and evolving stoichiometry such as in titration experiments (e.g.[80]) in solution during nucleation events.

Neutral ion pairs. The simulations conducted in this study revealed a consistent trend in the association energy among the studied dissolved complexes (in descending order: $CaCO_3^0$, $BaCO_3^0$, $BaSO_4^0$, and $CaSO_4^0$), which aligns with previous literature (Table 4) and with thermodynamic data (a.o. the phreeqc.dat database from PHREEQC, a computer program to preform aqueous geochemical calculations[81]). Additionally, the association energy values for ion pairs containing SO_4 ions were within the experimental ranges reported in the literature (Table 4). Notably, our force field and methodology led to a closer agreement with the experimental values for the association constant for $BaSO_4$ than a previous study,[28] where they used unbiased MD simulations that can lead to insufficient sampling of the different states and therefore a less accurate outcome.[28,82] For ion pairs containing CO_3 ions, a difference of only 1.6 kJ/mol was observed in the association energy values compared to experimental values. This difference is considered negligible as it falls below the thermal energy at ambient conditions (k_bT) and is significantly smaller than the variability observed in the experimental measurements. One possible explanation for this minor discrepancy is that the experimental free energies were determined using binding equilibria, where ion pairs could be part of a pre-nucleation cluster.[83] The experimental approach involved computing a weighted average of the free energy of isolated ion pairing and corresponding values within the complex environment, considering all possible association numbers and states of association.[69] In contrast, our simulations calculated the free energy for a single ion pair in aqueous solution. Previous MD simulations of $CaCO_3^0$ ion pairing,[22,69] reported similar association energies for $CaCO_3^0$ and the corresponding CTICs compared to our values (Table 4).[69] In general, we observed a higher association constant of neutral IPs, therefore the driving force for IP association is stronger compared to CTIC. Moreover, in most cases is the lifetime also longer, increasing the probability of further ion (pair) attachment and formation of critical nuclei, in agreement with our DLS results (Figure 6) and previous findings.[14]

Further structural implications. We compared the structural information obtained from the free energy profiles and surfaces with previously published experimental and computational observations. The structural arrangement of ion pairs can vary depending on factors such as ion size, charge, solvent nature, and ion concentration in solution.

In this study, the energy profile of $BaSO_4^0$ (Figure 5) indicated a slight preference for the bidentate configuration over the monodentate configuration. This contrasts with other MD simulations where they used a different forcefield, however that force field overestimated K_a^∞ with almost 3 orders of magnitude.[84] Conversely, our findings revealed that the IPs and CTICs with carbonate coordinate preferentially in the monodentate configuration. This observation aligns with first principles calculations that indicate the most stable coordination of carbonate with alkaline earths occurs in a monodentate fashion.[35] The energy profiles of $CaSO_4^0$ demonstrated that the monodentate configuration is again the most stable form, consistent with previously published MD simulations.[85]

The energy well depths and related configurations for the different CTICs also reflect their crystal structures. For instance, $BaSO_4$ has the most profound bidentate energy well (Figure 4c and Figure 5), which is known to transform into 100% bidentate coordination in its crystal structure (barite).[86,87] Calcite, the most stable crystal form of $CaCO_3$, exclusively exhibits monodentate configurations,[88] as seen here for the most stable configuration in the free energy profile of the dissolved neutral IP. $CaSO_4^0$ also display significant bidentate energy wells (Figure 5), albeit less profound than $BaSO_4^0$, which might explain the mix of mono- and bidentate coordination known for this system.[89] For gypsum, the most stable crystal structure of $CaSO_4$ at 300 K,[90] two SO_4^{2-} ions have bidentate coordination to Ca^{2+}, while two SO_4^{2-} are in monodentate configuration.[91] The stability of the $Ca-SO_4$ SIP configurations, compared to the mono-CIP (Figure 4c and Figure 5), likely reflects association and subsequent incorporation of structural water molecules as observed in the hydrated gypsum structure ($CaSO_4.2H_2O$).

Our findings emphasize once more that the impact of non-stoichiometric conditions should be taken into consideration when investigating dissolved complexes and ionic mineral formation under natural conditions. It is likely equally relevant in the development of inhibitors to prevent scale formation

where charged particles,[20] formed under non-stoichiometric conditions, show a different interaction with inhibitors.[92]

Conclusions

Molecular dynamics (MD) simulations and dynamic light scattering (DLS) flow experiments show that nucleation correlates with the stability and lifetime of the initial complexes, which were significantly impacted by the cation:anion stoichiometry and ion type. This in turn affects nucleation timing and particle size evolution: the stability and lifetime of the initial complexes correlate with particle formation as observed in experiments. Specifically, $Ba(SO_4)_2^{2-}$ was found to have higher association constants and its lifetime was twofold longer than $Ba_2SO_4^{2+}$, corresponding to larger particles in the DLS for the negative CTIC compared to the positive CTIC. For $CaCO_3$, the opposite trend was observed where $Ca(CO_3)_2^{2-}$ was found to have lower association constants and its lifetime was shorter than $Ca_2CO_3^{2+}$, matching with a lower probability for nucleation reflected by the observation of smaller particles at $r_{aq}=0.01$. The crosslinked systems, $BaCO_3$ and $CaSO_4$, showed similar trends as observed for $BaSO_4$. For the contribution of the individual ions, CTIC in systems with barium have a smaller association constant and a shorter lifetime compared to systems with calcium. In general, carbonate containing systems have a larger association constant, but a shorter lifetime compared to sulfate containing systems. Our results emphasize the impact of non-stoichiometric conditions on the first steps of nucleation in natural systems and indicates how this might affect the nucleation and growth of ionic mineral.

List of abbreviations

Abbreviation

bi-biCIP	Both ions in bidentate CIP configuration
CIP	Contact ion pair
CTIC	Charged triple ion complexes
DLS	Dynamic light scattering
DRS	Dielectric relaxation spectroscopy
FES	Free energy surfaces
IAP	Ion activity product
IP	Ion pair
IS	Ionic strength
MD	Molecular dynamics
mono-biCIP	One ion in monodentate and one ion bidentate configuration
mono-monoCIP	Both ions in a monodentate CIP configuration
RDF	Radial distribution function
SIP	Solvent shared ion pair
SSIP	Solvent separated ion pair

Frequently used symbols		**Unit**
$a_{cation/anion}$	Activity of cation or anion	–
K_a^{∞}	Association constants at infinite dilution	–
$\Delta G_a^{\ddagger}$	Association energy barriers	kJ/mol
$-\Delta G_a$	Association free energies	kJ/mol
k_a	Association rate constant	s^{-1}
Ω	Degree of supersaturation: IAP/Ksp	–
$\Delta G_d^{\ddagger}$	Dissociation energy barriers	kJ/mol
k_d	Dissociation rate constant	s^{-1}
r_{aq}	Initial ratio of free cation activity over the free anion activity	–
$K_{a2+/-}$	Positive (+) or negative (−) CTIC association constants, ion activity corrected	–
$-\Delta G_{a2+/-}$	Positive (+) or negative (−) CTIC association free energies	kJ/mol
A′	Pre-factor	s^{-1}
K_{sp}	Solubility product	–

Equation symbols

γ	Activity coefficient	–
γ_i^{EDH}	Activity coefficient after extended Debye-Hückel correction	–
k_b	Boltzmann constant	$m^2\ kg/s^2/K^1$
z_i	charge number of ion species I	–
λ_D	Debye length	m
a_i	Effective diameter of hydrated ion in angstroms	Å
q	Electric charge	C
c	Electrolyte concentration	Mol/L
$\Delta G(r)$	Free energy as a function of r	J
R	Gas constant	J/Mol/K
V°	Individual ionic volumes	L
V_{intr}	Intrinsic volume of electrolyte	m^3
RU	Maximum distance of the associated state	m^3
ε_{ms}	Molten salt dielectric constant	–
ε_0	Permittivity in vacuum	–
r	Radial distance	m
$g^{id}(r)$	Radial distribution function	

$a_{\ominus}$	Reference surface (10–20 m2)	m^2
C_s	Salt concentration	Mol/L
K_s	Setschenow coefficient	–
κ_T	Solvent isothermal compressibility	GPa^{-1}
$c^{\ominus}$	Standard state concentration (6.022×10^{26} Molecules per m3)	Molecules/m^3
T	Temperature	K
α	Total excess polarization parameter	L/mol
$\varepsilon_r(c)$	Water dielectric constant as a function of the electrolyte concentration	–

Funding

This project has received funding from the European Research Council (ERC) under the European Union's Horizon 2020 research and innovation programme (grant agreement No. 819588).

Conflict of Interests

The authors declare no conflict of interest. The funders had no role in the design of the study; in the collection, analyses, or interpretation of data; in the writing of the manuscript, or in the decision to publish the results.

Data Availability Statement

The data that support the findings of this study are available from the corresponding author upon reasonable request.

[1] A. Declet, E. Reyes, O. M. Suárez, *Reviews on Advanced Materials Science.* **2016**, *44*, 87–107.
[2] M. Claverie, M. Diez-Garcia, F. Martin, C. Aymonier, *Chem. Eur. J.* **2019**, *25*, 5814–5823.
[3] G. A. Tribello, F. Bruneval, C. C. Liew, M. Parrinello, *J. Phys. Chem. B* **2009**, *113*, 11680–11687.
[4] L. G. Benning, G. A. Waychunas, *Kinetics of Water-Rock Interaction* (Eds.: S. Brantley, J. Kubicki, A.White), Springer, New York, **2008**, 259–333.
[5] C. B. Whitehead, R. G. Finke, *Cite this: Mater. Adv.* **2021**, *2*, 186.
[6] D. G. Castellini, G. R. Dickens, G. T. Snyder, C. D. Ruppel, *Chem. Geol.* **2006**, *226*, 1–30.
[7] L. A. D. of W. and P. LADWP, "Mono Lake Mineral Water Quality," **n.d.**
[8] School of Ocean and Earth Sciences and Technology Hawaii (SOEST), **2017**.
[9] J. Kang, J. N. Bracco, J. D. Rimstidt, G. H. Zhu, F. Huang, C. Zhu, *Geochim. Cosmochim. Acta* **2022**, *317*, 180–200.
[10] L. Griffiths, M. J. Heap, F. Wang, D. Daval, H. A. Gilg, P. Baud, J. Schmittbuhl, A. Genter, *Geothermics.* **2016**, *64*, 235–245.
[11] L. T. MacHale, R. G. Finke, *Ind. Eng. Chem. Res.* **2023**, *62*, 9639–9661.
[12] M. Chaussemier, E. Pourmohtasham, D. Gelus, N. Pécoul, H. Perrot, J. Lédion, H. Cheap-Charpentier, O. Horner, *Desalination.* **2015**, *356*, 47–55.
[13] S. Y. M. H. Seepma, B. W. M. Kuipers, M. Wolthers, *ACS Omega.* **2023**, *8*, 5760–5775.
[14] S. Y. M. H. Seepma, S. E. Ruiz-Hernandez, G. Nehrke, K. Soetaert, A. P. Philipse, B. W. M. Kuipers, M. Wolthers, *Cryst. Growth Des.* **2021**, *21*, 1576–1590.
[15] V. M. Fokin, A. S. Abyzov, A. M. Rodrigues, R. Z. Pompermayer, G. S. Macena, E. D. Zanotto, E. B. Ferreira, *Acta Mater.* **2019**, *180*, 317–328.
[16] K. Larsen, K. Bechgaard, S. L. S. Stipp, *Geochim. Cosmochim. Acta* **2010**, *74*, 558–567.
[17] G. Nehrke, Calcite Precipitation from Aqueous Solution: Transformation from Vaterite and Role of Solution Stoichiometry, Utrecht University **2007**.
[18] M. Kowacz, C. V. V. Putnis, A. Putnis, *Geochim. Cosmochim. Acta* **2007**, *71*, 5168–5179.
[19] M. Wolthers, G. Nehrke, J. P. Gustafsson, P. Van Cappellen, *Geochim. Cosmochim. Acta* **2012**, *77*, 121–134.
[20] S. Y. M. H. Seepma, B. W. M. Kuipers, M. Wolthers, *ACS Omega.* **2023**.
[21] Y. Marcus, *Ions in Solution and Their Solvation*, John Wiley & Sons, Inc, Hoboken, NJ **2015**.
[22] P. Raiteri, A. Schuitemaker, J. D. Gale, *J. Phys. Chem. B* **2020**, *124*, 3568–3582.
[23] R. Buchner, T. Chen, G. Hefter, *J. Phys. Chem. B* **2004**, *108*, 2365–2375.
[24] W. W. Rudolph, G. Irmer, G. T. Hefter, *Phys. Chem. Chem. Phys.* **2003**, *5*, 5253.
[25] Y.-H. Zhang, C. K. Chan, *J. Phys. Chem. A* **2002**, *106*, 285–292.
[26] T. Chen, G. Hefter, R. Buchner, *J. Solution Chem.* **2005**, *34*.
[27] D. Schröder, L. Ducháčková, J. Tarábek, M. Karwowska, K. J. Fijalkowski, M. Oncák, P. Slavícek, *J. Am. Chem. Soc.* **2011**, *133*, 2444–51.
[28] F. Jones, S. Piana, J. D. Gale, *Cryst. Growth Des.* **2008**, *8*, 817–822.
[29] J. Corzo, M. Santamaria, *Biochem. Mol. Biol. Educ.* **2006**, *34*, 413–416.
[30] S. Plimpton, *J. Comput. Phys.* **1995**, *117*, 1–19.
[31] W. G. Hoover, *Phys. Rev. A* **1985**, *31*, 1695–1697.
[32] S. Nosé, *J. Chem. Phys.* **1984**, *81*, 511–519.
[33] Y. Wu, H. L. Tepper, G. A. Voth, *J. Chem. Phys.* **2006**, *124*, 024503.
[34] P. Raiteri, J. D. Gale, D. Quigley, P. M. Rodger, *J. Phys. Chem. C* **2010**, *114*, 5997–6010.
[35] P. Raiteri, R. Demichelis, J. D. Gale, *J. Phys. Chem. C* **2015**, *119*, 24447–24458.
[36] E. H. Byrne, P. Raiteri, J. D. Gale, *J. Phys. Chem. C* **2017**, *121*, 25956–25966.
[37] N. L. Allan, A. L. Rohl, D. H. Gay, C. R. A. Catlow, R. J. Davey, W. C. Mackrodt, *Faraday Discuss.* **1993**, *95*, 273.
[38] G. A. Tribello, M. Bonomi, D. Branduardi, C. Camilloni, G. Bussi, *Comput. Phys. Commun.* **2014**, *185*, 604–613.
[39] A. A. Chialvo, P. T. Cummings, H. D. Cochran, J. M. Simonson, R. E. Mesmer, *J. Chem. Phys.* **1995**, *103*, 9379–9387.
[40] M. Eigen, K. Tamm, *Z. Elektrochem.* **1962**, *66*, 93–121.
[41] J. Aufort, P. Raiteri, J. D. Gale, *ACS Earth Space Chem.* **2022**, *6*, 733–745.
[42] G. Raabe, R. J. Sadus, *J. Chem. Phys.* **2011**, *134*, 234501.
[43] N. Gavish, K. Promislow, *Phys. Rev. E* **2016**, *94*, 1–7.
[44] J. B. Hasted, D. M. Ritson, C. H. Collie, *J. Chem. Phys.* **1948**, *16*, 1–21.
[45] D. Langmuir, *Aqueous Environmental Geochemistry*, Prentice Hall **1997**.
[46] J. Kielland, *J. Am. Chem. Soc.* **1937**, *59*, 1675–1678.
[47] W. F. McDevit, F. A. Long, *J. Am. Chem. Soc.* **1952**, *74*, 1773–1777.
[48] C. Bretti, R. M. Cigala, F. Crea, C. De Stefano, G. Vianelli, *Eur. J. Pharm. Sci.* **2015**, *78*, 37–46.
[49] H. Zhao, R. Dilmore, D. E. Allen, S. W. Hedges, Y. Soong, S. N. Lvov, *Environ. Sci. Technol.* **2015**, *49*, 1972–1980.
[50] Y. Marcus, *J. Mol. Liq.* **2006**, *123*, 8–13.
[51] Y. Marcus, H. Donald Brooke Jenkins, L. Glasser, *J. Chem. Soc. Dalton Trans.* **2002**, *20*, 3795–3798.
[52] F. J. Millero, *Chem. Rev.* **1971**, *71*, 147–176.
[53] Y. Marcus, *The Properties of Solvents*, Vol. 53, John Wiley & Sons, Chichester **1999**.
[54] O. Allnér, L. Nilsson, A. Villa, *J. Chem. Theory Comput.* **2012**, *8*, 1493–1502.
[55] J. P. Gustafsson, Visual Minteq v3.1, a free equilibrium speciation model, Department of Land and Water Resources Engineering (Stockholm), **2013**.
[56] L. N. Plummer, E. Busenberg, *Geochim. Cosmochim. Acta* **1982**, *46*, 1011–1040.
[57] R. E. Zeebe, D. A. Wolf-Gladrow, *E. Oceanography*, *Book Series, Elsevier, Amsterdam.* **2001**, *65*.
[58] C. W. Davies, T. Shedlovsky, *J. Electrochem. Soc.* **1964**, *111*, 85C.
[59] *Malvern Panalytical Ltd.2020a.* **2020**.
[60] W. Brown, *Dynamic Light Scattering: The Method and Some Applications*, Clarendon Press **1993**.

[61] R. Shaw, *Dynamic Light Scattering Training* **2014**.
[62] G. Nehrke, G. J. Reichart, P. Van Cappellen, C. Meile, J. Bijma, *Geochim. Cosmochim. Acta* **2007**, *71*, 2240–2249.
[63] C.-W. Tai, V. Narsimhan, *Soft Matter.* **2022**, *18*, 4613.
[64] P. Bots, L. G. Benning, J.-D. D. Rodriguez-Blanco, T. Roncal-Herrero, S. Shaw, *Cryst. Growth Des.* **2012**, *12*, 3806–3814.
[65] E. Busenberg, L. N. Plummer, *Geochim. Cosmochim. Acta* **1986**, *50*, 2225–2233.
[66] P. Benes, H. Selecka, *Radiochem. Radioanal. Lett.* **1973**, *13*, 339–348.
[67] A. R. Felmy, D. Rai, J. E. Amonette, *The Solubility of Barite and Celestite in Sodium Sulfate: Evaluation of Thermodynamic Data*, Vol. 19, Springer **1990**.
[68] C. Monnin, *Chem. Geol.* **1999**, *153*, 187–209.
[69] M. Kellermeier, P. Raiteri, J. K. Berg, A. Kempter, J. D. Gale, D. Gebauer, *Wiley Online Library.* **2016**, *17*, 3535–3541.
[70] Z. Dai, A. Kan, F. Zhang, M. Tomson, J Chem Eng Data **2015, 60, 766-774**.
[71] R. M. Smith, A. E. Martell, *Critical Stability Constants*, Springer US, Boston, MA **1975**.
[72] D. Di Tommaso, N. H. de Leeuw, *Geochim. Cosmochim. Acta* **2009**, *73*, 5394–5405.
[73] F. S. Dukhovich, E. N. Gorbatova, M. B. Darkhovskii, V. K. Kurochkin, *Pharm. Chem. J.* **2002**, *36*, 248–254.
[74] J. R. Murdoch, *J. Chem. Educ.* **1981**, *58*, 32–36.
[75] A. E. Nielsen, *J. Cryst. Growth* **1984**, *67*, 289–310.
[76] S. L. Cumberland, G. F. Strouse, Langmuir. **2002, 18, 269-276**.
[77] J. J. De Yoreo, P. G. Vekilov, *Rev. Mineral. Geochem.* **2003**, *54*, 57–93.
[78] D. Kashchiev, *J. Chem. Phys.* **2007**, *127*, 64505.
[79] A. E. S. Van Driessche, M. Kellermeier, L. G. Benning, D. Gebauer (Eds.), *New Perspectives on Mineral Nucleation and Growth*, Springer, **2017**.
[80] D. Gebauer, A. Völkel, H. Cölfen, *Science* **2008**, *322*, 1819–1822.
[81] D. L. Parkhurst, C. A. J. Appelo, *Description of Input and Examples for PHREEQC Version 3 – A Computer Program for Speciation, Batch-Reaction, One-Dimensional Transport, and Inverse Geochemical Calculations* **2013**.
[82] A. Laio, M. Parrinello, *Proc. Natl. Acad. Sci. USA* **2002**, *99*, 12562–12566.
[83] R. M. Fuoss, T. Shedlovsky, *J. Am. Chem. Soc.* **1957**, *79*, 3301–3303.
[84] D. M. Warren, *Molecular Dynamics Simulations of Barite and Celestite Ion-Pairs* **2011**.
[85] R. P. Matthews, K. J. Naidoo, *J. Phys. Chem. B* **2010**, *114*, 7286–7293.
[86] S. E. Redfern, S. C. Parker, *J. Chem. Soc. Faraday Trans.* **1998**, *94*, 1947–1952.
[87] M. Miyake, I. Minato, … H. M.-A., undefined 1978, *pubs.geoscienceworld.orgM Miyake, I Minato, H Morikawa, S IwaiAmerican Mineralogist, 1978 pubs.geoscienceworld.org.* **n.d**.
[88] S. M. Antao, I. Hassan, *Can. Mineral.* **2010**, *48*, 1225–1236.
[89] S. M. Antao, I. Hassan, *Can Mineral.* **2009**, *47*, 1245–1255.
[90] D. Freyer, W. Voigt, *Monatsh. Chem.* **2003**, *134*, 693–719.
[91] J. C. A. Boeyens, V. V. H. Ichharam, *Z Krist - New Cryst St.* **2014**, *217*, 9–10.
[92] Z. Dai, Y. Zhao, S. Paudyal, X. Wang, C. Dai, S. Ko, W. Li, A. T. Kan, M. B. Tomson, SPE J. **2022**.

Manuscript received: November 20, 2023
Accepted manuscript online: December 8, 2023
Version of record online: February 20, 2024